result of the simple treatment will hold. Note, this schematic analysis assumes spin-orbit interactions to be present, so that angular-momentum conservation does *not* force $l_z = 0$ only.

Specific dynamical models imply various levels (or combinations of levels) of the hierarchy. Lin[7] has calculated the integrated cross section for the process analogous to Eq. (1) in Ar. He considers the Coulomb coupling between the channels $\alpha = 3$ and $\alpha = 7$, but he neglects spin-orbit coupling, and hence the channels i, altogether. This (together with initial-state correlations) is apparently adequate for the integrated cross section, but will require some extension to include spin-orbit effects to treat the angular distribution. The only calculation of the angular distribution of process (1) known to us is the one by Walker and Waber,[14] who obtain the value $\beta = 1.7$ at 304 Å, in the approximation of Eq. (13), using the Dirac-Slater model. The discrepancy may represent deficiencies in the Dirac-Slater model, or effects of channel interaction either within the ^2S manifold or with the $^2P^\circ$ channels as well,[7] or indeed other effects, such as initial-state correlations,[7] which would affect the amplitudes D_α. Further theoretical work will be needed to resolve these questions.[15]

---

[1]In the semiclassical theory of photoionization, the radiation field induces oscillations in the spherically symmetric s charge distribution along the axis of oscillation of the electric vector of the light. Hence, relative to this axis, $l_z = 0$.

[2]In general, both the orientation and magnitude of the electronic orbital momentum can be changed by anisotropic interactions. However, in the present example, conservation of angular momentum and parity force $l = 1$ only.

[3]For a general discussion see D. Dill, in *Photoionization and Other Probes of Many-Electron Interactions*, NATO-ASI Series, Series B, edited by F. J. Wuilleumier (Plenum, New York, 1976), pp. 387–394.

[4]D. Dill, Phys. Rev. A **7**, 1976 (1973).

[5]D. Dill and U. Fano, Phys. Rev. Lett. **29**, 1203 (1972).

[6]U. Fano and D. Dill, Phys. Rev. A **6**, 185 (1972).

[7]See, e.g., C. D. Lin, Phys. Rev. A **9**, 171, 181 (1974).

[8]J. L. Dehmer, to be published.

[9]See, e.g., J. L. Dehmer, W. A. Chupka, J. Berkowitz, and W. T. Jivery, Phys. Rev. A **12**, 1966 (1975).

[10]J. A. R. Samson and J. L. Gardner, Phys. Rev. Lett. **33**, 671 (1974).

[11]U. Fano, J. Opt. Soc. Am. **65**, 979 (1975).

[12]U. Fano and C. M. Lee, Phys. Rev. Lett. **27**, 1573 (1973).

[13]We set $D_j = (ns_{1/2}\epsilon p_j, J = 1 \| T^{[1]} = z \| n s_{1/2} n s_{1/2}, J_0 = 0)$ and apply twice Eq. (15.7') of U. Fano and G. Racah, *Irreducible Tensorial Sets* (Academic, New York, 1959).

[14]T. E. H. Walker and J. T. Waber, J. Phys. B **7**, 674 (1974).

[15]A similar analysis has been introduced in Ref. 4 to account for deviations from $\beta = 2$ in the process $Hg(5d^{10}6s^2\,^1S_0)$ → $Hg^4(5d^{10}6s\,^2S_{1/2})$ measured by A. Niehaus and M. W. Ruf, Z. Phys. **252**, 84 (1972), where the interaction is with discrete members of the p and f Rydberg series converging to the $Hg^+(5d^96s^2\,^2D_{5/2,\,3/2})$ ion states.

Absorption of Focused Light by Spherical Plasmas*

J. J. Thomson, C. E. Max, J. Erkkila, and J. E. Tull
University of California, Lawrence Livermore Laboratory, Livermore, California 94550
(Received 21 June 1976)

For light focused on spherical plasmas, we obtain new results giving the power absorbed by inverse bremsstrahlung and resonance absorption as a function of the focusing scheme. For a given beam profile and lens, there is an optimum focus to maximize total absorption. Linearly polarized beams lead to asymmetric absorption. Good agreement with experimental absorption and scattered light data is obtained.

Much of the theory of light absorption by plasma has been restricted to the case of plane waves incident on a plane-stratified slab. However, current laser fusion experiments involve the illumination of glass microspheres by highly focused light. We show that there are major consequences of this geometry on the magnitude and symmetry of absorption, which are important for the design and interpretation of laser fusion experiments. We demonstrate a focusing strategy which opti-

mizes laser light absorption by spherical targets. These theoretical predictions are consistent with experimental data on glass microspheres. Knowledge of our optimum focusing curve can be of considerable help in maximizing thermonuclear yield.

Our derivation consists of the following steps. First, we calculate the electromagnetic fields due to a focused beam separately in plasma and in vacuum. Then, by matching these two solutions at the plasma-vacuum interface, we establish an analogy between solutions for a spherical plasma and the known solutions for a planar plasma. Finally, we compute absorption in a spherical plasma, and show its dependence on parameters of the focused beam.

We assume that the laser light is axisymmetric and linearly polarized. First we consider the vacuum field,[1] which is determined by two potential functions χ and ψ satisfying the scalar wave equation:

$$(\nabla^2 + k^2)\begin{pmatrix} \chi \\ \psi \end{pmatrix} = 0. \tag{1}$$

The free space wave number is $k \equiv \omega/c$. Radial field components are related to χ and ψ by

$$\begin{pmatrix} E_r \\ B_r \end{pmatrix} = \frac{1}{ik}\left(\frac{\partial^2}{\partial r^2} + k^2\right)\begin{pmatrix} r\chi \\ r\psi \end{pmatrix}. \tag{2}$$

Note that E_r depends only on χ and B_r only on ψ. Other field components are sums of terms depending on either χ or ψ. Thus the total field is the sum of two modes, one dependent only on χ (the "transverse magnetic" or TM) and one dependent only on ψ (the "transverse electric" or TE). By analogy to plane waves, the TM mode is polarized in the plane of incidence ($B_r = 0$) and the TE mode is polarized perpendicular to the plane of incidence ($E_r = 0$).

We may solve Eq. (1) as follows:

$$\begin{pmatrix} \chi \\ \psi \end{pmatrix} = \sum_{l=0}^{\infty} a_l h_l^{(2)}(kr)P_l^1(\cos\theta)\begin{pmatrix} \cos\varphi \\ \sin\varphi \end{pmatrix}, \tag{3}$$

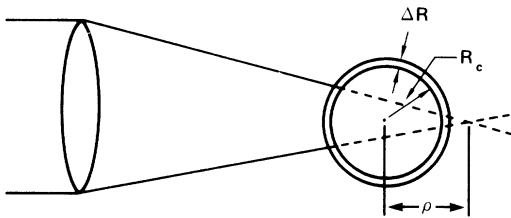where θ is the polar angle, measured relative to

the center of the spherical target, and φ is the azimuthal angle, measured relative to the polarization vector. P_l^1 is the Legendre function, and $h_l^{(2)}$ is the spherical Hankel function. The coefficients a_l (which may be complex) are functions of the light intensity profile at the lens, lens f number, spherical aberrations, and (since we place the center of our coordinate system at the the target center, see Fig. 1) the distance ρ between target center and lens geometric focus. For a complete description of the determination of a_l, the reader is referred to Erkkila[2] or Richards and Wolf.[3]

The power in each l mode is

$$P_l = (c/2k^2)l^2(l+1)^2(2l+1)^{-1}a_l a_l^*. \tag{4}$$

As an example, we show in Fig. 2(a) the l spectrum for an $f/2.5$ lens, for various displacements ρ of the target center from best focus. The light intensity profile at the lens is $I = I_0\exp[-(r/r_0)^5]$. We neglect spherical aberrations, which would make the spectra for positive and negative l's unequal.

Next we consider the fields inside the plasma. We assume a cold plasma and allow for a finite electron-ion collision frequency ν.[4] If the plasma is spherically symmetric, we may expand the potential functions as

$$\begin{pmatrix} \chi \\ \psi \end{pmatrix} = \sum_l \begin{pmatrix} \chi_l(r) \\ \psi_l(r) \end{pmatrix}P_l^1(\cos\theta)\begin{pmatrix} \cos\varphi \\ \sin\varphi \end{pmatrix} \tag{5}$$
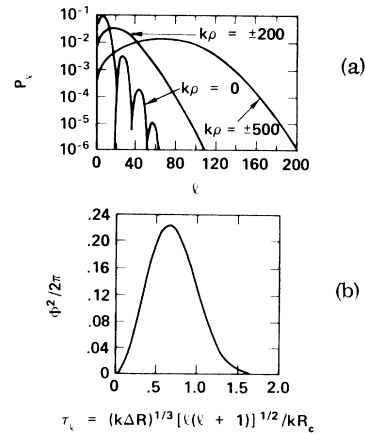

(a)

(b)

$$\tau_l = (k\Delta R)^{1/3}[l(l+1)]^{1/2}/kR_c$$

FIG. 2. (a) Power in each l mode, versus displacement ρ of target center from best focus. $k = \omega/c$.
(b) Fractional absorption of each l mode.

FIG. 1. Geometry of the focusing system.

and find that in the plasma χ_l and ψ_l satisfy

$$\left[\frac{d^2}{dr^2} - \frac{1}{\epsilon}\frac{d\epsilon}{dr}\frac{d}{dr} + k^2\left(\epsilon - \frac{l(l+1)}{k^2r^2}\right)\right](r\chi_l) = 0, \quad (6)$$

$$\left[\frac{d^2}{dr^2} + k^2\left(\epsilon - \frac{l(l+1)}{k^2r^2}\right)\right](r\psi_l) = 0. \quad (7)$$

Here $\epsilon \equiv 1 - (\omega_p^2/\omega^2)(1 + i\nu/\omega)^{-1}$.

Now consider a plane wave incident on a planar plasma with incidence angle θ_0, and density gradient in the z direction. If we write the magnetic field as $B = G(z)\exp[i(\omega t - ky\sin\theta_0)]$, then $G(z)$ satisfies[5]

$$\left[\frac{d^2}{dz^2} - \frac{1}{\epsilon}\frac{d\epsilon}{dz}\frac{d}{dz} + k^2(\epsilon - \sin^2\theta_0)\right]G(z) = 0 \quad (8)$$

for a wave polarized in the plane of incidence. Equations (8) and (6) are identical if one makes the equivalence $\sin^2\theta_0 \rightarrow l(l+1)/k^2r^2$. The latter term is nearly constant if $\Delta R \ll R_c$, where ΔR is the plasma gradient length, and R_c the radius of the critical density. This criterion is satisfied for many cases of interest. A similar equivalence holds for Eq. (7), with waves polarized perpendicular to the plane of incidence.

Next, we assume the plasma density profile is linear in order to obtain the most straightforward analytic results. To obtain the fields in the plasma due to the TM mode, we define $\alpha_l = [l(l+1)]^{1/2}/kR_c$, $r\chi_l = \beta G$ (β is a normalizing constant) and

$$-\eta \equiv \epsilon(r) = 1 - (\Delta R)^{-1}(R_c + \Delta r - r)(1 + i\nu/\omega). \quad (9)$$

To the left of the reflection point ($\eta = -\alpha_l^2$),

$$G(\eta) = (\pi\gamma/2)^{1/2}\exp(-i\pi/12)$$

$$\times(S/S')^{1/2}H_{1/3}^{(1)}(iS) + \text{c.c.}, \quad (10)$$

where $\gamma = k\Delta R$ ($\gg 1$), $S = \frac{2}{3}\gamma(\eta + \alpha_l^2)^{3/2}$, and $H_{1/3}$ is the Hankel function of order $\frac{1}{3}$. To obtain β, we equate the vacuum field to the plasma field at the plasma's edge, $\eta = -1$. We use the asymptotic expansions for $h_l^{(2)}$ and $H_{1/3}$, to evaluate the ingoing radial electric fields just inside and outside the plasma. We find

$$\chi_l = (a_l/kr)(1 - \alpha_l^2)^{1/4}G(\eta)\exp(i\delta), \quad (11)$$

where $\delta = -k(R_c + \Delta R) + \frac{2}{3}\gamma(1 - \alpha_l^2)^{3/2} + l\pi/2$. It is straightforward to evaluate all the TM fields in the plasma.

Now we are in a position to calculate the energy absorbed by resonantly driven fields. The absorbed energy is

$$P_{abs} = \int \nu(\langle E_r^*E_r\rangle/8\pi)r^2dr \sin\theta\, d\theta\, d\varphi. \quad (12)$$

Since the radial fields are peaked near critical

density,

$$E_r \cong l(l+1)(i\epsilon k^2r^2)^{-1}a_l(1 - \alpha_l^2)^{1/4}$$

$$\times P_l^1(\cos\theta)\cos\varphi\exp(i\delta)G(0). \quad (13)$$

Ginzburg[5] shows that

$$|G(0)|^2 \cong \Phi^2(\tau_l)(2\pi\gamma\alpha_l^2)^{-1}, \quad (14)$$

where $\tau_l = (k\Delta R)^{1/3}\alpha_l$ and $\Phi^2/2\pi$ is a function shown graphically in Fig. 2(b). Using Eqs. (13) and (14) in (12), we find that the fractional absorption of the lth TM mode is

$$f_{ra}^l = \pi^{-1}\Phi^2(\tau_l)(1 - \alpha_l^2)^{1/2}. \quad (15)$$

Thus the total power absorbed from the beam due to resonance absorption is

$$P_{abs} = \sum_l P_l(2\pi)^{-1}\Phi^2(\tau_l)(1 - \alpha_l^2)^{1/2}, \quad (16)$$

where P_l is the power in both the TE and TM lth mode.

Next, we describe the variation of total absorption with ρ, the distance of target center from best focus. Comparing Fig. 2(a) with Fig. 2(b), we see that for $k\rho = 0$, most of the light energy is in low l modes (i.e., nearly normal angles of incidence) which are not efficiently absorbed. At very large $k\rho$, the energy disperses to very high l modes, which are not efficiently absorbed because their turning points are too far from R_c. Therefore, the absorption curve has a maximum at some intermediate $k\rho$. This behavior is shown in the solid line of Fig. 3. In general, the $k\rho$ value for maximum absorption varies with f number, target size, and ΔR. The peak of the curve is broader for larger f numbers.

The experimental points on Fig. 3 represent absorption data for spherical glass targets. They
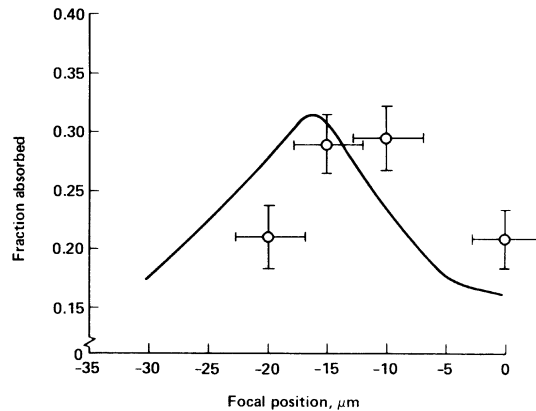
FIG. 3. Absorption versus target displacement from best focus. Solid curve is theory. Experimental points are from Ref. 6.

were taken from Ref. 6, which contains a full de-
scription of the experiments. Briefly, a 1.06-μm
Nd-glass laser system was used to illuminate
D-T filled hollow glass spheres, having 65–70 μm
diameter and 0.5–0.6 μm wall thickness. The fo-
cusing optics consisted of an $f/0.2$ elliptical mir-
ror pair. Figure 3 shows that both the magni-
tude and general shape of the absorption curve
are very well predicted. If the solid curve were
shifted sideways by 5 μm, experimental and theo-
retical values would agree almost perfectly. Such
a 5 μm displacement could represent uncertainty
in the position of best focus, or effects of depar-
ture from spherical symmetry. A more exten-
sive discussion of the absorption calculation (sol-
id curve) will appear elsewhere.

Solutions for the TE mode may be found as
above, and give the usual Airy functions. Of
course, the TE mode is not resonantly absorbed,
but both the TE and TM modes are absorbed by
inverse bremsstrahlung, which we now consider.
It is a well-known result that for a plane wave in-
cident at an angle θ_0 on a planar plasma, the
fractional absorption is

$$f_{ib} = (\tfrac{16}{15}) k \Delta R (\nu/\omega) \cos^5\theta_0, \tag{17}$$

where ν/ω is evaluated at the critical density,
and $f_{ib} \ll 1$ is the one way absorption. It is clear
from the WKB solutions of Eqs. (6) and (7), valid
away from the turning point, that Eq. (17) holds
for the focused case if one makes the substitution
$\theta_0 = \sin^{-1}[l(l+1)/k^2 R_c^2]^{1/2}$. Thus for focused
beams

$$f_{ib}{}^l = (\tfrac{16}{15}) k \Delta R (\nu/\omega) [1 - l(l+1)(kR_c)^{-2}]^{5/2}. \tag{18}$$

The total energy absorbed by both inverse brems-
strahlung and resonance absorption may be calcu-
lated using Eqs. (15) and (18). Comparing this
prescription to the numerical results of Ref. 2,
we find accuracy to order $\Delta R/R_c \ll 1$, which is
our expansion parameter.

A consequence of the asymmetry imposed by
linear polarization is that resonance absorption
is concentrated in lobes in the upper and lower
hemispheres (Fig. 4). This dependence can be
seen in the equation for $\langle E_r^2 \rangle$, Eq. (13). The
lobes correspond to rays polarized in the local
plane of incidence, which are resonantly ab-
sorbed. This asymmetry in absorption may lead
to asymmetries in compression of microspheres,
and to large thermoelectric magnetic fields due
to the nonuniform heating. The lobe pattern must
be taken into account in the design of illumination
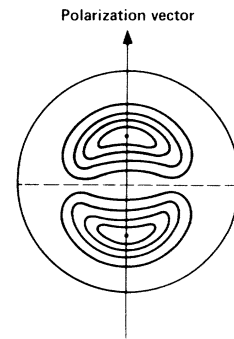schemes intended to heat spheres uniformly.

FIG. 4. Spatial dependence of relative power ab-
sorbed by resonance absorption. Each contour inter-
val represents 0.2 of the maximum.

As a result of the lobe structure of absorption
shown in Fig. 4, the scattered or nonabsorbed
laser light will have a polarization dependence.
The scattered light is predicted to be weaker in
the plane of polarization than out of it, because
more light is absorbed in the plane of polariza-
tion. Such an asymmetry in scattered light has
been observed in experiments.[6,7] These data are
a strong indication of resonance absorption, al-
though it must be noted that Brillouin sidescatter
may produce similar scattered light distributions
under some circumstances.

A basic assumption in the foregoing analysis
was that the plasma is spherically symmetric.
This may not hold well for one- or two-sided il-
lumination of spheres, or for very intense light
($\gtrsim 10^{15}$ W/cm^2) where the effects of nonlinear self-
steepening and critical surface rippling become
important.

In summary, we have shown that resonance ab-
sorption of linearly polarized focused light is
concentrated in two lobes aligned along the polar-
ization vector. The scattered light is predicted
to be a maximum in the plane perpendicular to
the polarization vector. Absorption is maxi-
mized by focusing somewhat off the center of a
spherical target, the amount being a function of
lens and target parameters.

We wish to thank Alex Glass and W. L. Kruer
for informative discussions, and Erik Storm for
sharing his data with us.

[1]M. Born and E. Wolf, *Principles of Optics* (Perga-
mon, New York, 1975).
[2]J. Erkkila, Ph.D. thesis, University of California

Report No. UCRL-51914, 1974 (unpublished).

[3]B. Richards and E. Wolf, Proc. Roy. Soc. London Ser. A 253, 358 (1959).

[4]Total absorption is proportional to the area under the resonance curve, and is thus insensitive to the value of ν. For a discussion of hot plasma effects on res-

onance absorption, see D. W. Forslund et al., Phys. Rev. A 11, 679 (1975), and references therein.

[5]V. L. Ginzburg, Propagation of Electromagnetic Waves in Plasmas (Pergamon, New York, 1964).

[6]K. R. Manes et al., to be published.

[7]W. C. Mead et al., Phys. Rev. Lett. 37, 489 (1976).

Effect of Acoustoelectric Phonons on Anomalous Transmission of X Rays*

S. D. LeRoux,† R. Colella, and R. Bray

Physics Department, Purdue University, West Lafayette, Indiana 47907

(Received 3 May 1976)

Acoustoelectrically amplified phonon beams were used to attenuate anomalous transmission of x-rays in InSb at 77°K. It is found that anomalous transmission is a very sensitive probe for phonon detection. The mean square atomic displacement and the associated strain produced by the intense phonon beam can be accurately determined. Weakly enhanced phonon modes other than those predicted by the acoustoelectric theory have also been detected using this x-ray technique.

The feasibility of using x-ray diffraction for investigating acoustoelectrically amplified phonon beams in InSb has been recently demonstrated by symmetric Bragg reflection from the (00h) planes.[1] It has been shown that symmetric satellites of various orders develop on the wings of the diffraction peaks. Some accompanying attenuation of the central elastic peak was interpreted as due to an enhancement of the Debye-Waller factor produced by the phonon beam.

In this paper, the Laue case of diffraction (transmission) has been used, with $21 \le \mu t \le 32$ (μ is the linear absorption coefficient; t is the thickness of the crystal).[2] When μt is large (> 10), x rays can propagate through the crystal by means of anomalous transmission (A.T.), which is very sensitive to any kind of lattice disturbances, including atomic vibrations.[3,4] Our objective was to look for a decrease in A.T. by acoustoelectrically amplified phonons under circumstances similar to those described in Ref. 1. A noticeable decrease of A.T. is expected with mean acoustic fluxes that would not be detectable by the Bragg reflection technique. The present experiments and the Bragg diffraction experiments are complementary. From the angular position of the satellites in the latter we determined the phonon wave vectors and deduced the frequency spectrum of the amplified phonons. From the attenuation in A.T. we can evaluate the atomic vibrational amplitude u, and hence the strain, due to the integrated amplified phonons, by interpreting the attenuation of the elastic diffraction peak as due to an "enhanced" Debye-Waller factor.[4] This procedure is much more accurate and reli-

able than that used in reflection experiments.[1]

A double-crystal technique in the parallel arrangement $(n, -n)$ was used, with a monochromator in the Bragg reflecting position, and the second crystal (the sample) set for Laue diffraction. Anomalous transmission of Mo-$K\alpha$ x rays ($\lambda = 0.711$ Å) was measured in n-type InSb single crystals with thicknesses ranging from 1.00 to 1.55 mm. The crystals were cut in the form of rectangular bars, with length (20–25 mm) along [110] and side faces (001) and (1$\bar{1}$0). dc electric field pulses were applied along the [110] direction to produce[1] an intense flux of [110] fast transverse acoustic phonons, polarized along [001]. These phonons are preferentially amplified from the thermal equilibrium background by the acoustoelectric interaction. The latter process is optimized by immersing the sample in liquid nitrogen for efficient cooling, and applying transverse magnetic fields. The diffracting planes were parallel to [110] and perpendicular to the lateral face (2–3 mm wide) on which the x-ray spot (2×0.5 mm^2) impinged. The amplified phonons are polarized along [001], parallel to the reciprocal lattice vector $\vec{G}$ for the (004) reflection for A.T., and have the maximum scattering effect on the x rays.

The same pulse technique illustrated in Ref. 1 was used, whereby the electric field was applied every other pulse and the output from the x-ray detector (a proportional counter) was switched back and forth between two sections of a multichannel analyzer, so that two rocking curves could be recorded simultaneously during the same run, one with phonons on and the other with